has reported the T_p data for several intermetallics. However, since the $-\Delta H_e$ values of the oxide of vanadium cannot be "adjusted" for every composition of Al–V compounds, one is obliged to lump the T_p values for all Al–V compounds. As argued above, a general trend in Fig. 1 is quite clear, in that metals whose oxides have low $-\Delta H_e$ values (e.g. Ni) give intermetallics with high T_p values whereas the opposite obtains for metals such as La, the oxide of which has a very high $-\Delta H_e$ value.

In Fig. 2, appropriate data on the intermetallic compounds of Zn with four metals are presented and the various quantities have the same significance as in Fig. 1. Once again one observes that metals such as Cu (whose oxide has a low $-\Delta H_e$ value) give intermetallics with high T_p values whereas those with relatively high values of $-\Delta H_e$ for the oxides (e.g. Mn) tend to impart low T_p values to the intermetallics.

It is realized that the conceptual basis for Figs. 1 and 2 can be discussed very qualitatively only. However, it is clear that Figs. 1 and 2 provide a rough guide line for the prediction of the effect on the T_p of a series of intermetallics formed by combining one metal with a series of other metals.

References

1. H. E. N. STONE, *J. Mater. Sci.* **9** (1974) 607.
2. *Idem, ibid* **7** (1972) 1147.
3. A. K. VIJH, *ibid* **5** (1970) 379.
4. *Idem*, "Electrochemistry of Metals and Semiconductors" (Marcel Dekker, New York, 1973) Ch. 1.
5. R. T. SANDERSON, "Chemical Periodicity" (Reinhold, New York, 1960); *idem*, "Inorganic Chemistry" (Reinhold, New York, 1967).

Received 29 August
and accepted 9 October 1974

ASHOK VIJH
Hydro-Quebec Institute of Research,
Varennes, P.Q.,
Canada

Vacancy ordering in cobalt sulphide

Although the structure of cobalt sulphide (CoS) is nominally of the NiAs-type, the compound does not exist at the stoichiometric one-to-one atomic ratio but is found within a limited range of composition near $CoS_{1.15}$. In view of the cobalt deficiency it is expected that ordering of the cobalt atoms and vacancies would occur, similar to that observed in other transition metal sulphur systems, e.g. Cr–S [1], Fe–S [2].

Various compositions of cobalt sulphide were prepared by direct combination of the elements at 1000° C in sealed silica tubes. After annealing at different temperatures, thin foils for examination in a JEM 200 electron microscope were prepared by grinding the specimens in a mortar and collecting the fragments on a copper grid. The electron diffraction patterns from specimens annealed below 450° C (Fig. 1) show the presence of extra reflections besides those characteristic of an NiAs-type cell. All the reflections could be indexed in terms of an hexagonal supercell with dimensions,

$$a_s = 2a_h, c_s = 3c_h,$$

where the subscripts h and s refer to the basic NiAs and superstructure cells respectively.

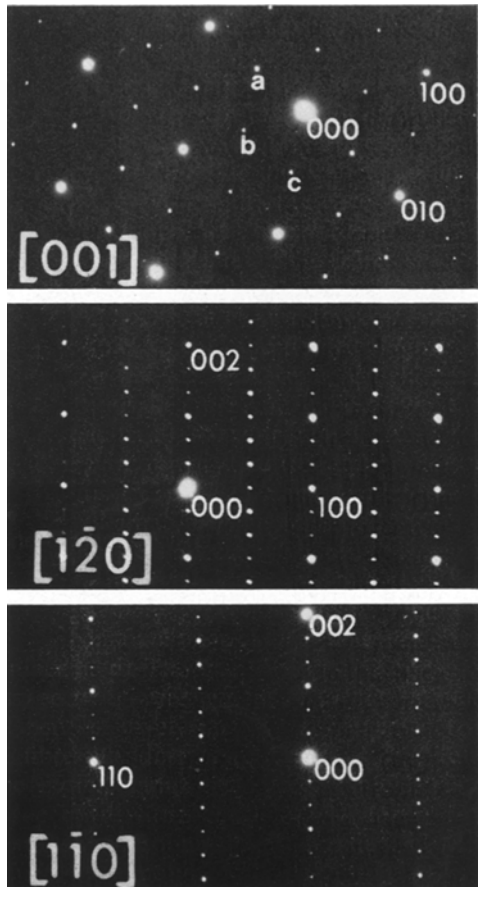

Figure 1 Electron diffraction patterns from Co_7S_8. Indices of reflections and beam directions refer to the basic NiAs-type cell.

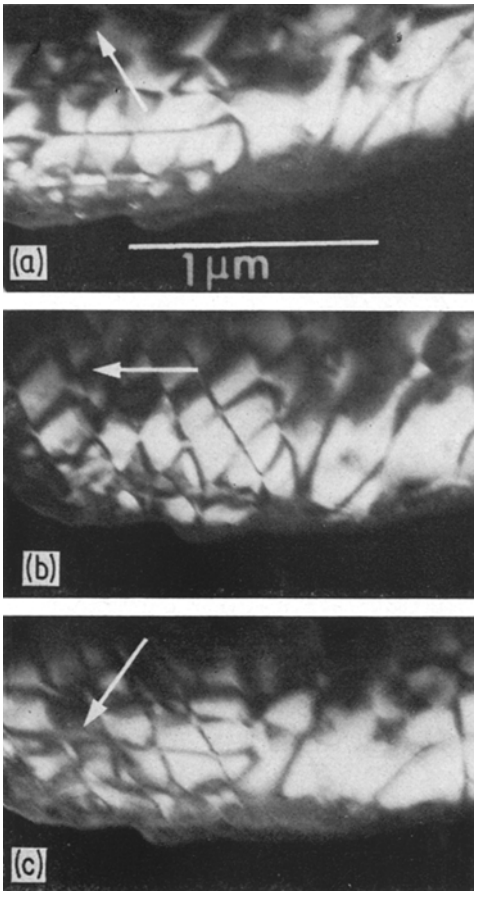

Figure 2 Hexagonal arrays of antiphase boundaries in Co_7S_8. Dark-field images recorded using the superlattice reflections marked (a), (b) and (c) in Fig. 1. Arrows indicate the direction of operating g-vector.

The type of vacancy ordering in this superstructure is similar to that found by Fleet [3] for Fe_7S_8. The vacancy positions in the unit cell are 0, $\frac{1}{2}$, 0; $\frac{1}{2}$, $\frac{1}{2}$, $\frac{1}{3}$; $\frac{1}{2}$, 0, $\frac{2}{3}$. Thus the cobalt atom layers perpendicular to the hexagonal *c*-axis are alternately fully and three-quarters occupied, with three vacancy containing layers required to define the projected positions of the vacancies onto the basal plane. Only one superlattice orientation may be distinguished by electron diffraction, although two enantiomorphic forms

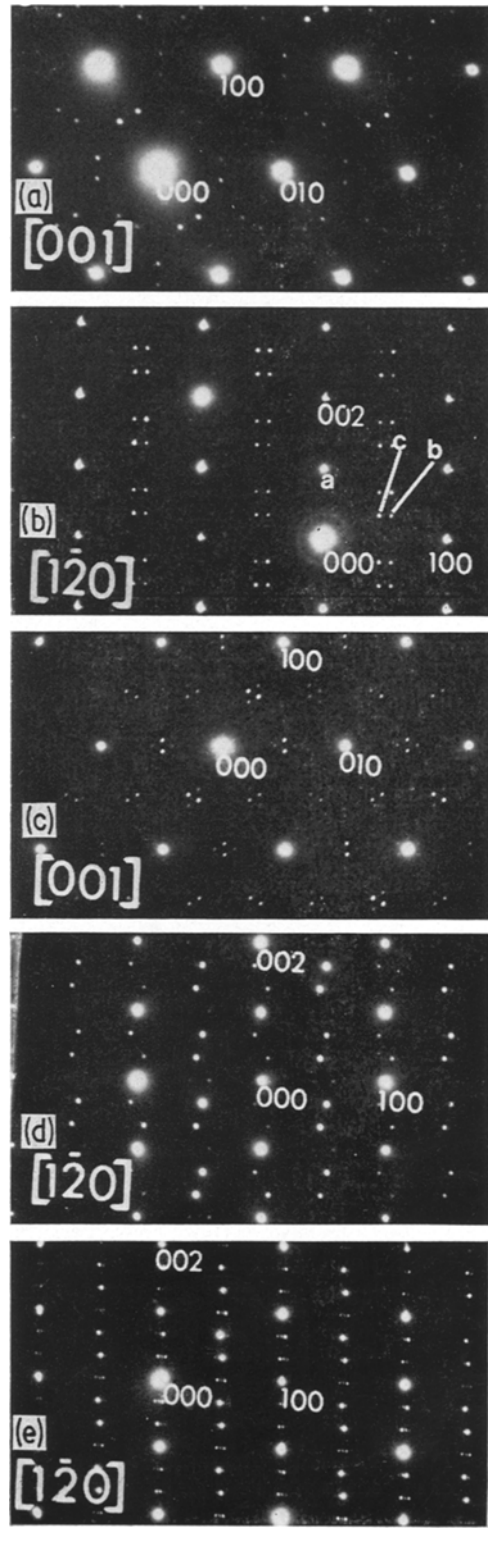

Figure 3 Electron diffraction patterns from long-period structures in cobalt sulphide. (a) and (b) from eleven-fold structure, in (b) both crystallographic variants contribute to pattern. (c) and (d) nineteen-fold structure. (e) forty-three-fold structure, some reflections from Co_7S_8 contribute to this pattern.

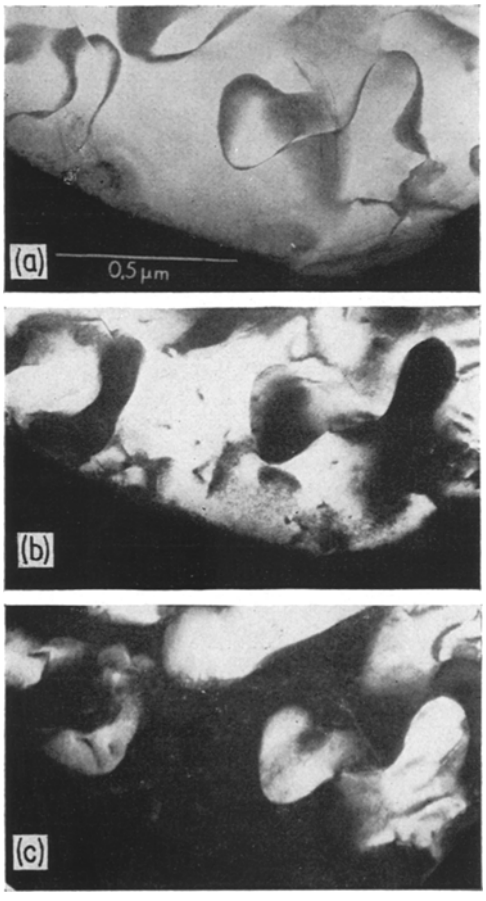

Figure 4 Dark-field images obtained from eleven-fold structure using the reflections marked (a), (b) and (c) in Fig. 3b. (b) and (c) are complementary images showing the two crystallographic variants, while the reflection used to form image (a) is common to both variants.

are possible belonging to space groups $P3_1$ and $P3_2$.

Planar boundaries forming hexagonal networks (with the c-axis as common zone) were frequently observed in Co_7S_8 as shown in Fig. 2. The criterion for boundary extinction $2\pi\mathbf{g}.R = 0,2\pi$, etc. (where $\mathbf{g}$ is the diffracting vector and R the lattice displacement associated with the boundary) indicated antiphase boundaries with displacement vectors perpendicular to the plane of the boundary. The atomic configuration of these boundaries shows that they are associated with a local excess or deficit of cobalt vacancies.

Within the approximate temperature ranges 850 to 750°C, 750 to 550°C and 550 to 450°C three different types of superstructure were found. The diffraction patterns from these superstructures (Fig. 3) could be indexed in terms of hexagonal (trigonal) cells with respective basal plane a_s parameters eleven, nineteen and forty three times that of the basic NiAs-type cell. The height of the unit cells remained $3c_h$ as in Co_7S_8. For each of the three superstructures two orientation variants related by a rotation of 180° (or 60°) about the c-axis could be distinguished by electron diffraction and dark-field imaging as shown in Fig. 4.

Although it has not yet been possible to determine the precise nature of the vacancy ordering in these superstructures, it would appear from the similarity in their diffraction patterns to those of Co_7S_8 that the arrangement of vacancies in the three partly filled cobalt atom layers (related to each other by the symmetry operations of space group $P3_1$ or $P3_2$) is based on the arrangement found in Co_7S_8. The splitting of certain reflections into pairs indicates that they are probably long-period structures, i.e. each partly filled layer contains a number of similar small groupings of vacancies separated by a two-dimensional network of antiphase boundaries.

In the superstructure with basal parameter eleven times that of the basic cell the absence of reflections of the type $h00$ ($0k0$, etc.) except where h is a multiple of eleven indicates that the total number of vacancies in the unit cell will be a multiple of three and eleven. The composition that satisfies this condition and is nearest to Co_7S_8 ($CoS_{1.142}$) is $Co_{627}Vac_{99}S_{726}$ ($CoS_{1.159}$). The origin of the hexagonal networks of antiphase boundaries (Fig. 2) may now be tentatively explained as the result of transforming the long-period structure (near the ideal $CoS_{1.159}$ composition) into Co_7S_8 after cooling below 450°C.

The observation of these superstructures with large unit cells over a range of compositions about $CoS_{1.142}$ indicates that they do not form in order to accommodate a small excess or deficit of cobalt vacancies into a new ordered structure, i.e. the formation of a particular superstructure is temperature rather than composition dependent. This is in contrast to the long-period structures in vanadium carbide [4], where the spacing of non-conservative antiphase boundaries follows the overall composition. The other possibility is that the origin of the superstructures may be explained in terms of the lowering in the electronic energy of the crystal due to the creation of new Brillouin zone boundaries near the Fermi surface. This explanation, originally

developed by Sato and Toth [5, 6] for Cu–Au alloys, has recently been found applicable to the two-dimensional long-period superstructures in hexagonal Cu–Sb [7] and Au–Cd [8] alloys. The low temperature instability of the long-period structures in cobalt sulphide, which is also quite common in metallic alloys, is thought to be due to the temperature dependence of the antiphase boundary energy.

References

1. F. JELLINEK, *Acta Cryst.* **10** (1957) 620.
2. E. F. BERTAUT, *ibid* **6** (1953) 557.
3. M. E. FLEET, *ibid* **B27** (1971) 1864.
4. M. H. LEWIS and J. BILLINGHAM, *Phil. Mag.* **29** (1974) 437.
5. H. SATO and R. S. TOTH, *Phys. Rev.* **127** (1962) 469.
6. *Idem*, "Alloying Behaviour and Effects in Concentrated Solid Solutions" (Gordon and Breach, New York, 1965) p. 295.
7. S. YAMAGUCHI and M. HIRABAYASHI, *J. Phys. Soc. Japan* **33** (1972) 708.
8. M. HIRABAYASHI, S. YAMAGUCHI, K. HIRAGA, N. INO, H. SATO and R. S. TOTH, *J. Phys. Chem. Solids* **31** (1970) 77.

Received 29 August
and accepted 5 September 1974

P. S. BELL*
Department of Physics,
University of Warwick, Coventry, UK

*Present address: Materials Division, Central Electricity Research Laboratories, Leatherhead, Surrey.

Large work of fracture values in wire reinforced, brittle-matrix composites

The purpose of this note is to draw attention to a feature of the pull-out of ductile fibres from brittle-matrix composite materials, which may lead to large values of the work of fracture of the composite.

In the course of an investigation into the pull-out of long metal wires from epoxy resin and cement matrices, the behaviour of work-hardened nickel wires was compared with that of annealed nickel wires of the same diameter. The experimental arrangement is shown in Fig. 1. A completely cracked matrix was simulated by dividing the cast resin at some point along the length of the wire with a thin flake of mica. A cement of epoxy resin matrix surrounding the wire was produced by casting cement or resin into a cavity machined in a resin block. This facilitated alignment of the wire and subsequent gripping of the specimen. The wires in the resin matrix were in general inclined at some angle $\pm\ \theta$ to the normal to the simulated crack but for brevity in this note we will describe only results for $\theta = 0$, i.e. with the wires normal to the simulated crack and parallel to the tensile stress during pull-out. Qualitatively, the comparison of the behaviour of cold-worked and annealed nickel wires described below for $\theta = 0$ holds for other values of θ, although variation of θ introduces significant quantitative variations, which will be described in another place.

In the pull-out tests, the work-hardened wire fractured when its shorter embedded length exceeded a critical value, whereas the annealed wire invariably pulled out of the matrix, even when its shorter embedded length was five times the critical length of the work-hardened wire (Fig. 2). To check that this difference did not arise from a change in the surface condition of the wire during annealing, the results of annealing in air and in argon and of etching the wire in acid after annealing were compared. These variations had no effect on the pull-out behaviour of the annealed wire. Closely similar results were obtained when the wires were embedded in a cement matrix (Fig. 3).

The force needed to pull an annealed nickel wire from a resin matrix as a function of the separation of the two halves of the specimen is shown in Fig. 4, for a wire of 55 mm shorter embedded length. The force remains constant (subject to minor fluctuations) for a substantial fraction of the total separation. Because of this feature, and because the length of wire embedded can be increased indefinitely without leading to

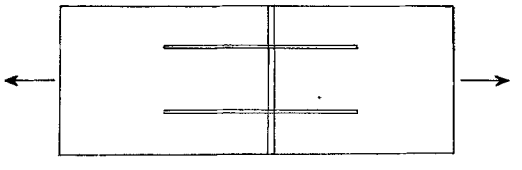

Figure 1 Specimen consisting of a pair of nickel wires embedded in an epoxy resin or cement matrix containing a simulated crack.